Nuclear Materials and Energy 45 (2025) 102035

Contents lists available at ScienceDirect

Nuclear Materials and Energy

journal homepage: www.elsevier.com/locate/nme

Paramagnetic radiation-induced defect centres and their correlation with the optical properties of irradiated advanced ceramic breeder pebbles

Andris Antuzevics [a], Guna Krieke [a], Jekabs Cirulis [a], Magdalena Rzepna [b], Maria Gonzalez [c], Julia M. Leys [d], Regina Knitter [d], Arturs Zarins [e,f,*]

[a] Institute of Solid State Physics, University of Latvia, 8 Kengaraga Str., LV-1063 Riga, Latvia
[b] Institute of Nuclear Chemistry and Technology, Centre for Radiation Research and Technology, Radiation Sterilization Plant for Medical Devices and Allografts, 16 Dorodna Str., 03-195 Warsaw, Poland
[c] LNF-CIEMAT, Materials for Fusion Group, Avenida Complutense 40, 28040 Madrid, Spain
[d] Karlsruhe Institute of Technology, Institute for Applied Materials, 76021 Karlsruhe, Germany
[e] University of Latvia, Faculty of Science and Technology, Institute of Chemical Physics, 1 Jelgavas Str., LV-1004 Riga, Latvia
[f] Daugavpils University, Faculty of Natural Sciences and Healthcare, Department of Environment and Technologies, 1A Parades Str., LV-5401 Daugavpils, Latvia

ARTICLE INFO

Keywords:
Tritium breeding
Advanced ceramic breeder pebbles
Paramagnetic radiation-induced defect centres
Optical absorption
Thermally stimulated luminescence

ABSTRACT

Advanced ceramic breeder (ACB) pebbles, primarily composed of lithium orthosilicate (Li_4SiO_4) with lithium metatitanate (Li_2TiO_3) as a second phase, are currently under development and testing as the European Union's reference material for tritium breeding in future thermonuclear fusion reactors. In the present work, the formation and accumulation of paramagnetic radiation-induced defect centres is investigated and compared for the first time in the untreated and thermally pre-treated ACB pebbles under exposure to different types of ionising radiation. Electron paramagnetic resonance (EPR) spectroscopy is employed, with particular focus on correlating the detected EPR signals with the optical properties of the irradiated pebbles. The stability of the radiation-induced optical absorption bands and the positions of the main peaks in the thermally stimulated luminescence (TSL) glow curves are correlated to the annealing of the EPR signals at $g = 2.04$ and $g = 2.00$. Within the same temperature range, transformations occur among various radiation-induced electron-type centres, originating from structurally related sites formed in the bulk of the material. The annealing of these electron-type centres proceeds in multiple stages up to 350 °C, involving recombination with hole-type centres that exhibit different stabilities. The obtained results highlight the important role of paramagnetic centres in determining the optical properties of the irradiated ACB pebbles.

1. Introduction

Advanced ceramic breeder (ACB) pebbles, primarily composed of lithium orthosilicate (Li_4SiO_4) with lithium metatitanate (Li_2TiO_3) as a second phase, have been designed and extensively tested as the European Union's reference material for tritium breeding in the helium cooled pebble bed (HCPB) blanket concept [1]. The HCPB concept is part of test blanket module (TBM) program within the international thermonuclear experimental reactor (ITER) project [2] and is also intended for application in the demonstration power plant (DEMO) [3]. Under operational conditions, the biphasic ACB pebbles will be subjected to extreme conditions, e.g., high-energy neutrons and other types of ionising radiation, elevated temperatures, strong magnetic fields, etc. Therefore, to investigate their *in-situ* tritium release behaviour under neutron irradiation at temperatures ranging from 400 to 900 °C, the ACB-TREND (**A**dvanced **C**eramic **B**reeder's in situ **T**ritium **R**elease **E**xperiment under **N**eutron irra**D**iation) campaign was recently initiated [4]. Although a limited number of short, preliminary neutron irradiation experiments have been conducted with various parameters, and the release behaviour of the generated tritium and helium by nuclear transmutation reactions of lithium with neutrons has been analysed in *in-situ* [5] and *ex-situ* modes [6], access to neutron irradiation facilities remains constrained. Consequently, alternative irradiation sources and ionising radiation of different types, masses, and energies have previously been applied in order to characterise radiation-induced effects in the untreated and thermally pre-treated ACB pebbles: (1) photons (X-

* Corresponding author at: University of Latvia, Faculty of Science and Technology, Institute of Chemical Physics, 1 Jelgavas Str., LV-1004 Riga, Latvia.
E-mail address: arturs.zarins@lu.lv (A. Zarins).

https://doi.org/10.1016/j.nme.2025.102035
Received 8 September 2025; Received in revised form 24 October 2025; Accepted 25 November 2025
Available online 26 November 2025

rays, gamma rays, and *bremsstrahlung*) with energies up to 6 MeV; (2) electrons (beta particles and accelerated electrons) with energies up to 10 MeV and irradiation temperatures up to 1000 °C; (3) accelerated ions with masses up to 127 amu (hydrogen, deuterium, helium, oxygen, silicon, argon, iron, and iodine) and energies up to 20 MeV [7,8]. It is well known that the interaction mechanisms and penetration depths of ionising radiation in matter depend on the mass, electric charge, and energy of the incident particles [9,10]. Therefore, by combining results from various irradiation studies, a comprehensive understanding of radiation-induced effects in the ACB pebbles can be achieved.

In the present work, the formation and accumulation of paramagnetic radiation-induced defect centres (containing unpaired electrons) is investigated and compared for the first time in the untreated and thermally pre-treated ACB pebbles under exposure to different types of ionising radiation using electron paramagnetic resonance (EPR) spectroscopy. Special emphasis is placed on understanding the correlation between the detected EPR signals and the optical properties of the irradiated ACB pebbles. Optical microscopy is commonly employed as one of the standard techniques for visual inspection and geometrical characterisation, including colour changes, of neutron-irradiated Li_4SiO_4 and Li_2TiO_3 pebbles [10,11]. The observed colour changes for Li_4SiO_4 (from "pearl" white to black/grey) and Li_2TiO_3 pebbles (from off-white to blue) after irradiation using neutrons at elevated temperatures (up to 850 °C) are probably related to the formation and accumulation of optically active radiation-induced defect centres (hereinafter referred to colour centres) that absorb ultraviolet–visible light. As part of this work, diffuse reflectance spectroscopy is used to analyse radiation-induced colour centres, while thermally stimulated luminescence (TSL) technique provides insights into the radiative recombination processes of electrons (e^-) and holes (h^+) trapped in radiation-induced defect centres in the irradiated ACB pebbles (resulting in emission of light with specific energy and wavelength) during heating. To directly compare the obtained results of EPR and diffuse reflectance spectroscopy with TSL data, the isochronal annealing method was applied, allowing to investigate annealing behaviour of radiation-induced defect centres with various properties as a function of temperature. Afterwards, these results can also be correlated with tritium release behaviour from the neutron-irradiated ACB pebbles, which has previously been analysed using thermal desorption spectrometry (TDS) [6].

2. Experimental

To investigate the influence of different types of ionising radiation on the formation and accumulation of paramagnetic centres (Table 1), the ACB pebbles with a nominal composition of 65 mol% Li_4SiO_4 and 35 mol % Li_2TiO_3 were fabricated using the melt-based process at the KALOS (**KA**rlsruhe **L**ithium **O**rtho**S**ilicate) facility [1]. Using powder X-ray diffractometry (PXRD, Bruker AXS Advanced) and inductively coupled plasma – optical emission spectrometry (ICP-OES, iCAP 7600 – ThermoFisher Scientific), it was confirmed that the fabricated pebbles consisted of 65.3 mol% Li_4SiO_4 (monoclinic form) and 34.7 mol% Li_2TiO_3 (cubic form). For irradiation using X-rays, the untreated pebbles were exposed at room temperature (20–25 °C) in air for 30 min to an X-ray source operated at a voltage of 45 kV and a current of 10 mA, resulting in an estimated absorbed dose of about 1 kGy. The dosimetry of the X-ray source was conducted using an RTI Piranha meter. For irradiation using accelerated electrons, the pebbles were inserted into a plastic bottle with dry air and subsequently sealed inside a vacuumed plastic bag. Afterwards, the irradiation was performed using 10 MeV accelerated electrons at the Institute of Nuclear Chemistry and Technology in Warsaw, Poland, with the "Elektronika 10/10" linear accelerator [12,13]. The process was carried out step-wise with 25 kGy increments, up to a total absorbed dose of about 0.5 MGy. The dosimetry was carried out using a graphite calorimeter according to ASTM 51631-20e1. During each irradiation cycle, the sample temperature remained below 50 °C, as determined by calorimetric measurements. For irradiation using accelerated ions, a pressed pellet with a diameter of about 13 mm and thickness of about 2 mm was used instead of the pebbles to allow easier handling and precise positioning during irradiation. Prior to irradiation, the prepared pellet was thermally pre-treated at 400 °C in vacuum to remove physisorbed and chemisorbed water (H_2O) vapour from the surface [14]. The thermally pre-treated pellet was then irradiated using 2.1 MeV H^+ ions at the Centre for Micro Analysis of Materials (CMAM) [15] in Madrid, Spain, under vacuum and without external heating, up to a total fluence of $5 \bullet 10^{16}$ ions/cm^2. It is expected that the surface irradiation temperature during irradiation remained below 100 °C. Penetration depth and damage profiles of accelerated ions were modelled using SRIM (**S**topping and **R**ange of **I**ons in **M**atter) software with full damage cascade simulations. Assuming a material density of about 2.5 g/cm^3 [1], the calculated penetration depth of 2.1 MeV H^+ ions in the pebbles was about 45 μm (Fig. 1). The total absorbed dose was estimated to be about 1.5 GGy and was calculated by dividing the deposited energy of accelerated ions by the mass of the irradiated pellet volume. Before characterisation using EPR spectroscopy, the irradiated

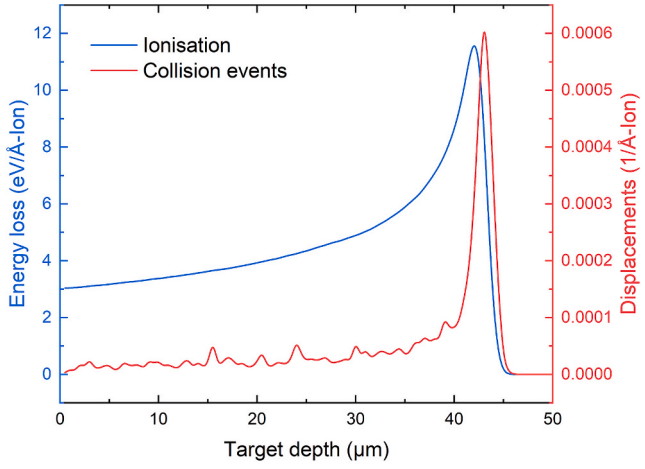

Fig. 1. SRIM plots for the distribution of ionisation losses and collision events in the untreated ACB pebbles induced by 2.1 MeV H^+ ions.

Table 1
Summary of irradiation conditions for the untreated and thermally pre-treated ACB pebbles exposed to different types of ionising radiation.

Applied type of ionising radiation	Description of irradiated sample	Sample shape	Irradiation conditions	Penetration depth	Measurement time
Up to 45 keV X-rays	Un-treated ACB pebbles (65 mol% Li_4SiO_4 and 35 mol% Li_2TiO_3) Thermally pre-treated ACB pebbles (70 mol % Li_4SiO_4 and 30 mol% Li_2TiO_3)	Pebbles (250 – 1250 μm size)	~1 kGy, 20-25 °C, air	Entire pebble volume	Immediately after the irradiation
10 MeV accelerated electrons	Un-treated ACB pebbles (65 mol% Li_4SiO_4 and 35 mol% Li_2TiO_3)	Pebbles (250 – 1250 μm size)	~0.5 MGy, ≤50 °C, dry air	Entire pebble volume	~1 year after the irradiation
2.1 MeV H^+ ions	Un-treated ACB pebbles (65 mol% Li_4SiO_4 and 35 mol% Li_2TiO_3)	Pressed pellet (~13 mm diameter, ~2 mm thickness)	~1.5 GGy, ≤100 °C, vacuum	≤45 μm depth	~5 years after the irradiation

pellet was carefully crushed into fine powder using an agate mortar at room temperature in air to ensure sample homogenisation. EPR spectra of the untreated ACB pebbles were measured immediately after irradiation using X-rays, about 1 year after irradiation using accelerated electrons, and about 5 years after irradiation using accelerated ions. Since unstable paramagnetic centres decay over time at room temperature [16,17], the obtained EPR spectra were normalised before isochronal annealing, and the intensities of individual signals after annealing were compared to the initial spectra of the irradiated pebbles. Annealing was performed from room temperature up to 350 °C in a custom-built furnace with an estimated temperature uncertainty of ±10 °C, maintaining each annealing step for 10 min.

To investigate radiation-induced colour centres and their correlation to paramagnetic centres, the fabricated ACB pebbles with a nominal composition of 70 mol% Li_4SiO_4 and 30 mol% Li_2TiO_3 were used (Table 1). To obtain a crystalline phase composition and microstructure representative of operational conditions, the fabricated pebbles were thermally pre-treated at 900 °C for 24 h in air by a muffle furnace. According to previous studies [18], thermal pre-treatment above 700 °C prior to irradiation can influence the distribution of paramagnetic centres in the pebbles due to the reversible polymorphic phase transition of Li_4SiO_4 between 600 and 750 °C. Using ICP-OES and PXRD, it was confirmed that the thermally pre-treated pebbles consisted of 70.5 mol% Li_4SiO_4 (monoclinic form) and 29.5 mol% Li_2TiO_3 (monoclinic form). Afterwards, the thermally pre-treated pebbles were irradiated using an X-ray source operated at 45 kV and 10 mA for 30 min at room temperature in air, corresponding to a total absorbed dose of about 1 kGy. The exposure to X-rays was chosen due to the practical advantages of allowing immediate EPR spectra measurements following irradiation, which is crucial for detecting unstable paramagnetic centres [16,17]. After irradiation, the pebbles were stored at room temperature in air for up to 8 days, and characterisation was conducted at selected time intervals. Annealing was performed immediately after the irradiation from room temperature up to 350 °C.

EPR spectroscopy investigations of the irradiated ACB pebbles and crushed powder before and after annealing were conducted using a Bruker Elexsys-II E500 spectrometer. The EPR spectra were acquired at room temperature using 9.83 GHz frequency microwave radiation with 10 mW power, 100 kHz magnetic field modulation frequency, and 0.4 mT modulation amplitude. For EPR spectra simulations, the EasySpin software [19] integrated into a custom code was used.

Diffuse reflectance spectra were measured using a double-beam spectrophotometer Specord 210. The ACB pebbles were pressed into a pellet prior to irradiation using X-rays to ensure even light scattering in all directions during spectra measurements. The intensity of radiation-induced absorption was calculated by subtracting the diffuse reflectance signal before and after irradiation.

TSL glow curves and spectra were measured using the Lexsyg research TSL/OSL reader from Freiberg Instruments GmbH. Before each measurement, the ACB pebbles were preheated to 350 °C in the reader to eliminate previously formed radiation-induced defect centres. The pebbles were irradiated using X-ray source VF-50 J/S operated at 40 kV and 0.5 mA. The signals were detected by a photomultiplier tube R13456 from Hamamatsu and a DV420A-BU2 CCD camera coupled to an Andor SR-303i-B spectrometer. A 1 °C/s heating rate was used for TSL glow curve measurements.

3. Results and discussion

3.1. Influence of different types of ionising radiation

Fig. 2 compares the normalised EPR spectra of the untreated ACB pebbles subjected to different types of ionising radiation: (1) up to 45 keV X-rays (measured immediately after the irradiation); (2) 10 MeV accelerated electrons (about 1 year after the irradiation); (3) 2.1 MeV H^+ ions (about 5 years after the irradiation). The resulting EPR signals vary

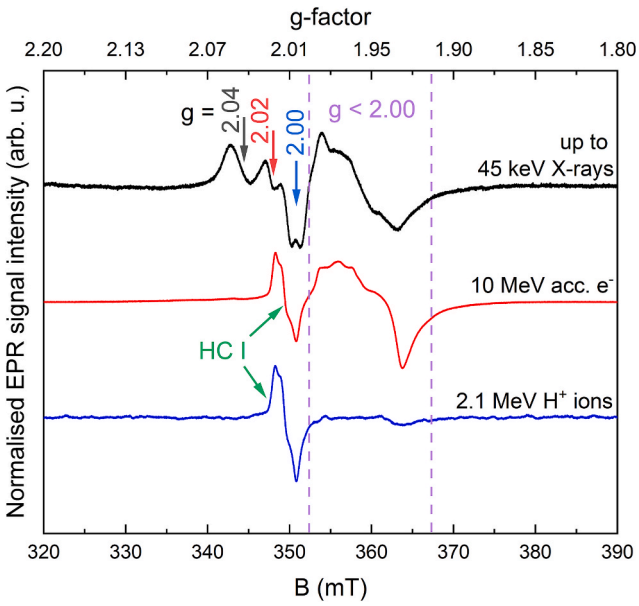

Fig. 2. Normalised EPR spectra of the untreated ACB pebbles after irradiation using different types of ionising radiation.

depending on the ionising radiation energy, penetration depth, absorbed dose, and the time elapsed since irradiation. Fig. 3 presents an alternative EPR spectra comparison with graded intensity scales to address discrepancies in the absorbed doses and times elapsed between irradiation and measurements. Both X-rays and accelerated electrons have the necessary energy to irradiate entire volume of the pebbles with a size distribution of 250–1250 μm, while in the case of accelerated ions, only the surface of the pressed pellet will be irradiated (up to about 45 μm depth). During irradiation using X-rays, the electrons and holes created by the indirect ionisation are trapped at both intrinsic (crystal lattice imperfections) and extrinsic (impurity-related) defect sites of the crystal structure forming paramagnetic centres. During irradiation using accelerated electrons, the formation of paramagnetic centres is induced by direct ionisation, electronic excitation (radiolysis), and single atomic displacements. During irradiation using accelerated ions, the ionisation losses (i.e., direct ionisation and radiolysis) are induced along particle penetration depth in the material, while matrix distortions due to collision events and atomic displacements are mainly at the stopping range of the implanted particles.

EPR signals formed in the untreated ACB pebbles following irradiation using X-rays are consistent with previous studies [16,18]. As the spectra were detected several minutes after the irradiation at room temperature, the least stable signals associated with trapped holes (labelled as $g = 2.04$ and $g = 2.02$) can still be detected. These paramagnetic centres anneal in the 25–100 °C range (Fig. 3(a) and (d)). The $g = 2.00$ region is constituted by several overlapping signals originating from the Li_4SiO_4 phase of the ACB pebbles [17]. These are usually attributed to trapped electrons in oxygen vacancies, based on the g-factor similarities to E'-type paramagnetic centres in quartz [20]. Additionally, a group of overlapping signals appears in the 352–367 mT ($g < 2.00$) range. The origin of these signals is still unclear; however, their formation has been suggested to be linked to electron-type centres (ECs) due to the trapping of titanium from the Li_2TiO_3 phase in the Li_4SiO_4 phase during the rapid solidification process of the ACB pebbles [21].

The EPR spectrum of the ACB pebbles after irradiation using accelerated electrons (Fig. 2) shows a higher signal-to-noise ratio but a smaller variety of EPR signals. The enhanced signal-to-noise ratio is attributed to the significantly higher absorbed dose during irradiation using accelerated electrons (about 0.5 MGy) compared to exposure

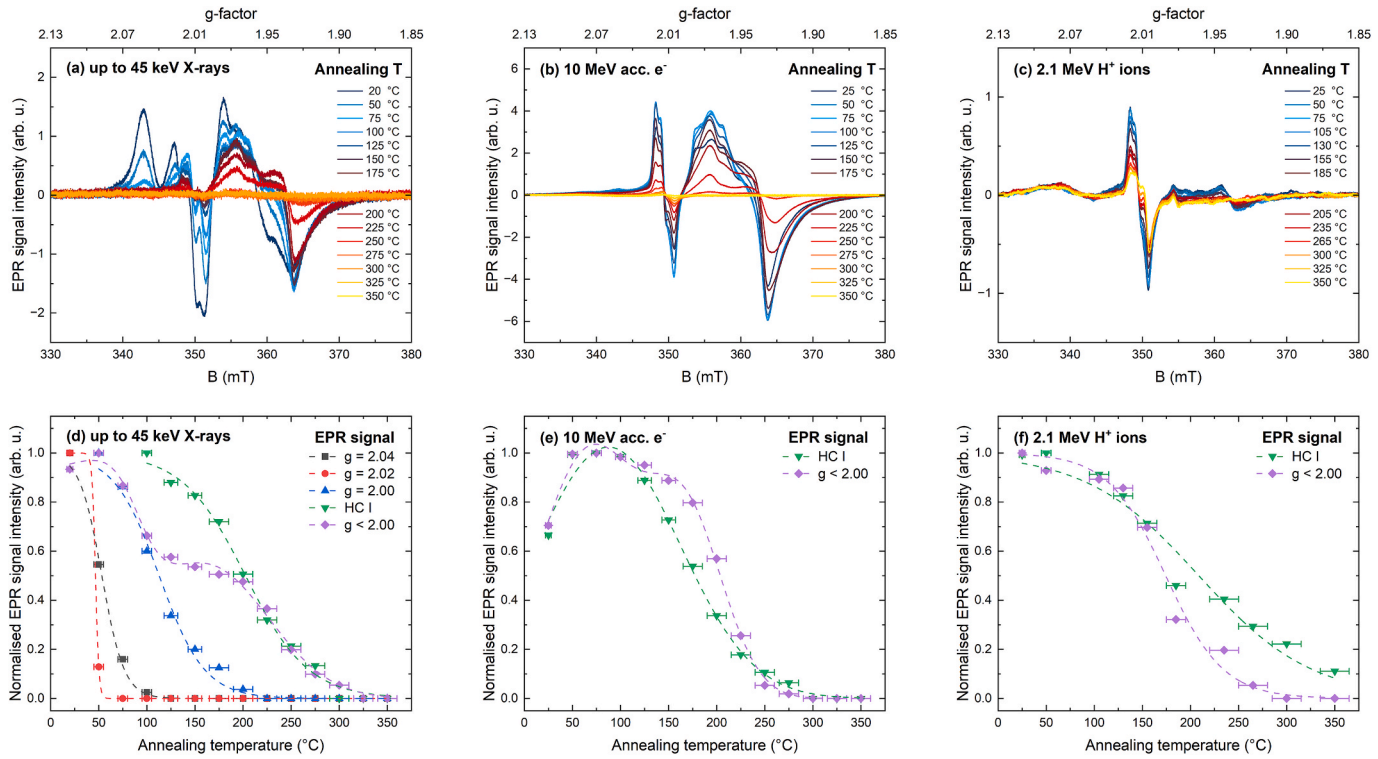

Fig. 3. EPR spectra and annealing kinetics of individual signals after irradiation of the untreated ACB pebbles using **(a)**, **(d)** up to 45 keV X-rays; **(b)**, **(e)** 10 MeV accelerated electrons; **(c)**, **(f)** 2.1 MeV H^+ ions.

using X-rays (about 1 kGy), resulting in a larger concentration of paramagnetic centres. However, as a result of the prolonged storage time of the accelerated electron-irradiated ACB pebbles prior to EPR spectra measurements, the less stable centres ($g = 2.04, 2.02, 2.00$) have already decayed. Consequently, only minor changes are observed for these pebbles after annealing in the 50–100 °C range (Fig. 3(b) and (e)). Instead, a rather synchronous decay of the stable hole-type centre (HC I) and $g < 2.00$ EPR signals occurs within the 125–250 °C annealing range. The annealing behaviour of these stable paramagnetic centres can be directly compared across different irradiation types and absorbed doses, regardless of time elapsed since irradiation. According to previous studies [16,17], the HC I signal originates from a hole trapped at an oxygen ion resulting in the formation of O^--type centre in the Li_4SiO_4 phase of the ACB pebbles during irradiation.

The penetration depth of accelerated ions is an important factor to consider when evaluating formation of paramagnetic centres in the ACB pebbles. Compared to X-rays and accelerated electrons, 2.1 MeV H^+ ions have a limited penetration depth (Fig. 1), resulting in a reduced irradiated volume and, consequently, a worse signal-to-noise ratio in the EPR spectrum (Fig. 2). Only the presence of stable paramagnetic centres is expected, given the extended storage time of the sample at room temperature. Notably, the HC I signal position and shape are essentially the same for both the accelerated ion- and electron-irradiated ACB pebbles. However, the generation efficiency of the $g < 2.00$ signals is significantly lower after irradiation using accelerated ions. This suggests that the formation of paramagnetic ECs occurs predominantly within the bulk volume of the ACB pebbles. As a result of a small irradiated volume in the case of accelerated ions, the $g < 2.00$ signals are weaker despite the higher absorbed dose (about 1.5 GGy).

A comparison of the annealing kinetics following irradiation with different types of ionising radiation (Fig. 3) provides additional insights into the accumulation and stability of ECs in the ACB pebbles. Three stages can be distinguished in the annealing kinetics of the $g < 2.00$ signals following irradiation using X-rays (Fig. 3(d)): (1) the initial decline 50–100 °C, likely associated with the annealing of the less stable $g = 2.04$ signal; (2) a subsequent decrease between 125–200 °C, correlated with the decay of $g = 2.00$ signal; (3) final stage at 200–300 °C, which overlaps with the annihilation of the HC I signal. In contrast, the $g < 2.00$ signal in both the accelerated electron- (Fig. 3(e)) and ion-irradiated ACB pebbles (Fig. 3(f)) shows a more gradual, monotonic decrease. This behaviour is consistent with the presence of only the more stable HC I signals in these samples. These observations support the interpretation that the complex $g < 2.00$ region arises from multiple overlapping EC signals, each with distinct thermal stabilities and suggest the existence of several recombination pathways. Additional details on the complex annealing behaviour of ECs in the thermally pre-treated ACB pebbles after irradiation using X-rays will be provided in Section 3.2 of the article.

3.2. Optical properties and their correlation to paramagnetic centres

Both paramagnetic and non-paramagnetic centres can contribute to the optical properties of the irradiated ACB pebbles. To investigate and compare the signals of radiation-induced defect centres with various properties, TSL glow curves and diffuse reflectance spectra were analysed. The TSL glow curve of the thermally pre-treated ACB pebbles after irradiation using X-rays (Fig. 4) consists of at least two overlapping peaks with maxima at 88 °C and 150 °C. The dominant signal in TSL spectra for these two peaks contains a broad luminescence band with a maximum at 408 nm. The changes in the local structure of the emitting centres could explain the decreased width of luminescence band for TSL peaks as the annealing temperature increases. The obtained results suggest the coexistence of several trapping and emitting centres in the irradiated pebbles. Similar emission spectra have been reported in Li_4SiO_4 associated with intrinsic point defects [22,23].

Diffuse reflectance spectra were measured (Fig. 5(a)) to characterise the formation of colour centres upon exposure of the thermally pre-treated ACB pebbles to X-rays. The diffuse reflectance spectra before irradiation consist of two dominant absorbance bands in the blue and green spectral ranges with maxima at 405 nm and 540 nm. Similar

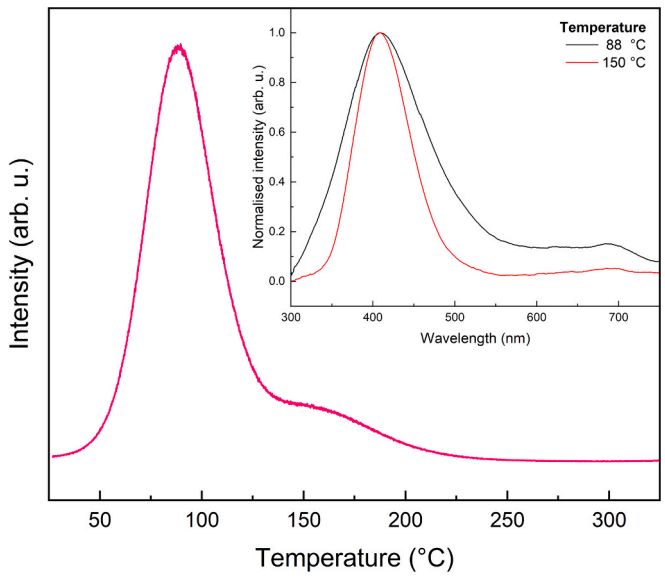

Fig. 4. TSL glow curve of the thermally pre-treated ACB pebbles after irradiation using X-rays; inset: TSL spectra detected at 88 °C and 150 °C.

absorption bands have been reported previously [22] and could be related to both intrinsic defects and impurity ions. After irradiation, an additional broad absorbance band was detected, indicating the formation of radiation-induced colour centres. After storage of the irradiated sample in darkness, a gradual decrease in intensity was detected, most likely due to thermal liberation of trapped mobile charge carriers in intrinsic and extrinsic defects.

Fig. 5(b) shows an analogous experiment monitoring the changes of radiation-induced EPR signals with time. Gradual decrease of $g = 2.04$ and $g = 2.00$ signals is observed, while the intensity of the signal in the $g < 2.00$ range increases, which is consistent with previous studies [16]. As shown in Fig. 6, the changes in the integral absorption intensity of radiation-induced colour centres are correlated with the $g = 2.00$ EPR signal.

Annealing of the irradiated ACB pebbles led to a reduction in the absorbance intensity of radiation-induced colour centres. Fig. 7(a) shows the changes in the diffuse reflectance spectra after annealing at different temperatures, while Fig. 7(b) illustrates the correlation between the TSL glow curve and the annealing behaviour of radiation-induced optical absorption and EPR signals. To evaluate the quantitative relationship between the integral radiation-induced optical absorption band and the EPR signal at $g = 2.00$, the Pearson correlation coefficient (PCC) was calculated between their temperature dependences. The resulting coefficient $r = 0.96$ indicates a strong positive correlation. Linear regression analysis (See Fig. S1 of the Supporting Information file) confirms that 92 % of the variance in the optical absorption can be explained by the EPR signal intensity. This supports the conclusion that both signals arise from the same radiation-induced defect centre.

A comparison of the annealing kinetics of individual EPR signals following irradiation using X-rays (Fig. 3(d) and Fig. 7(b)) reveals differences between the untreated and thermally pre-treated ACB pebbles. While slight compositional differences of the pebbles may contribute,

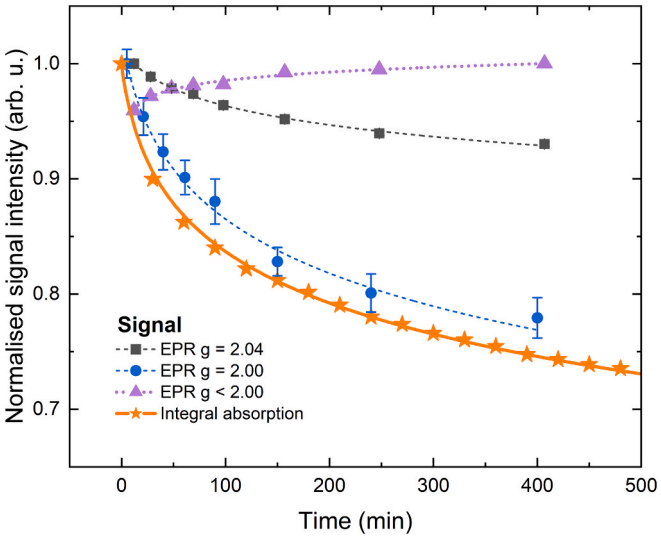

Fig. 6. Comparison of radiation-induced optical absorption and EPR signal stabilities for the thermally pre-treated ACB pebbles after irradiation using X-rays.

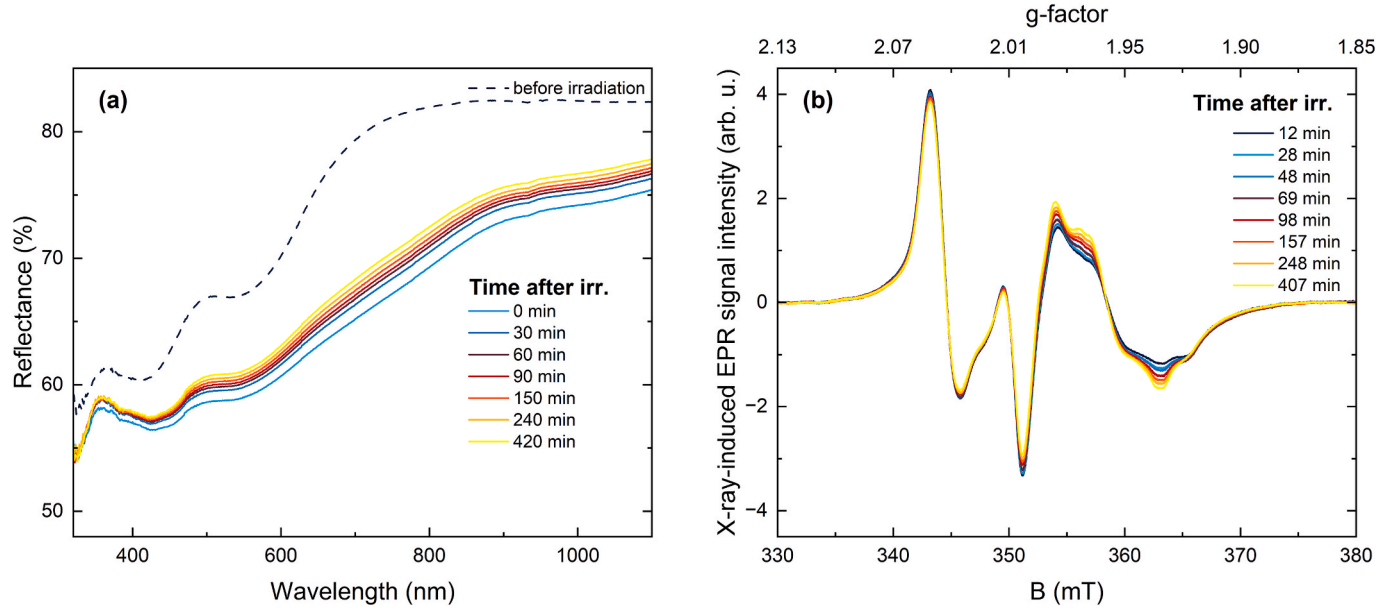

Fig. 5. **(a)** Diffuse reflectance and **(b)** EPR spectra of the thermally pre-treated ACB pebbles detected 0–420 min after irradiation using X-rays.

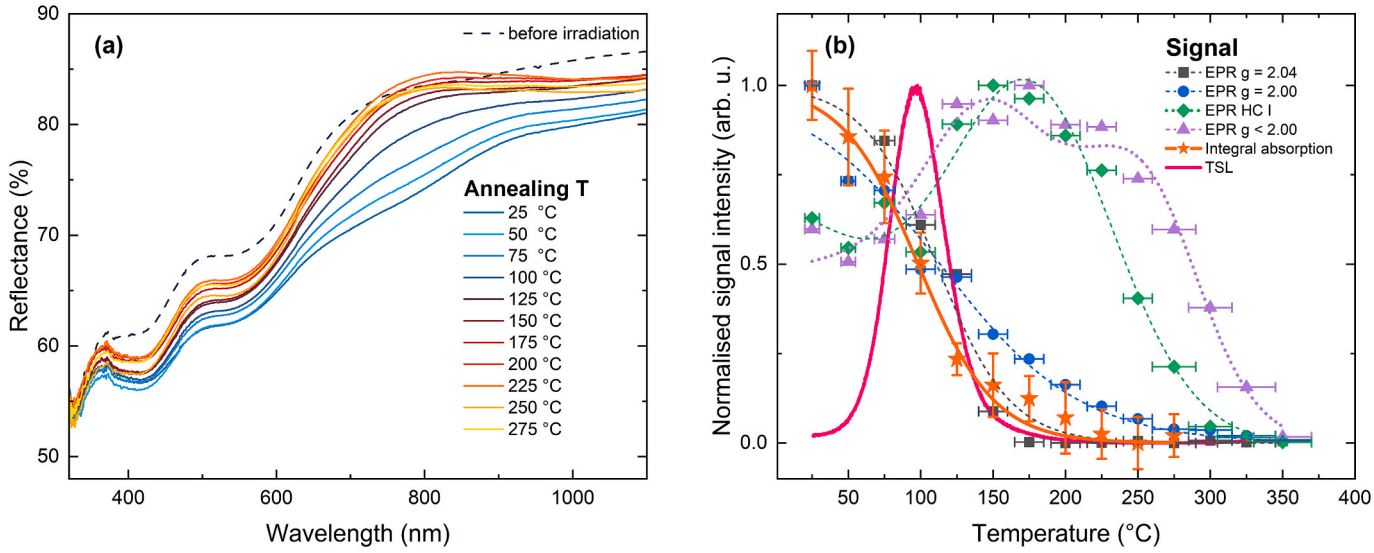

Fig. 7. **(a)** Diffuse reflectance spectra of the thermally pre-treated ACB pebbles detected after irradiation using X-rays and subsequent annealing; **(b)** TSL glow curve and annealing kinetics of the radiation-induced optical absorption and EPR signals.

the primary factor is associated with thermal pre-treatment prior to irradiation. Quantitatively, intensity variations of up to a factor of five for individual EPR signals of the generated paramagnetic centres have been reported [18]. Despite these differences, both untreated and thermally pre-treated pebbles exhibit similar EPR signals after irradiation using X-rays ($g = 2.04$, 2.00, HC I, and $g < 2.00$). In the thermally pre-treated pebbles, the paramagnetic centres anneal at slightly higher temperatures. The annealing kinetics of the $g = 2.04$ and $g = 2.00$ signals correlate with the thermal stability of the diffuse reflectance curve, and their rapid decline in the 25–150 °C range overlaps with the major peaks of the TSL glow curve (Fig. 4). These observations suggest that paramagnetic centres play a key role in determining the optical properties of the irradiated pebbles. However, these correlations do not necessarily mean that the paramagnetic centres themselves serve as the colour or recombination centres.

Multiple experimental observations and literature reports indicate the complex nature of the $g < 2.00$ signal. Notably, the signal structure varies significantly depending on the applied type of ionising radiation (Fig. 2). Additionally, changes in the spectral shape are observed upon annealing (Fig. 3) and during storage at room temperature over varying time intervals (Fig. 5(b)). Previous studies have attempted partial simulations of individual components contributing to the EPR spectrum in the $g < 2.00$ range [16,21].

Fig. 8 provides a solution based on EPR spectra simulations, which can account for the full thermal annealing behaviour of the $g < 2.00$ signal in the thermally pre-treated ACB pebbles after irradiation. The simulations were performed using the following spin-Hamiltonian:

$$H = g\mu_B BS \quad (1)$$

where g is the g-factor; μ_B – the Bohr magneton; B – external magnetic field; S – electronic spin operator [24]. The fitted principal g-factor values of individual components are listed in Table 2. Simulations of individual EC components after annealing of the irradiated pebbles are

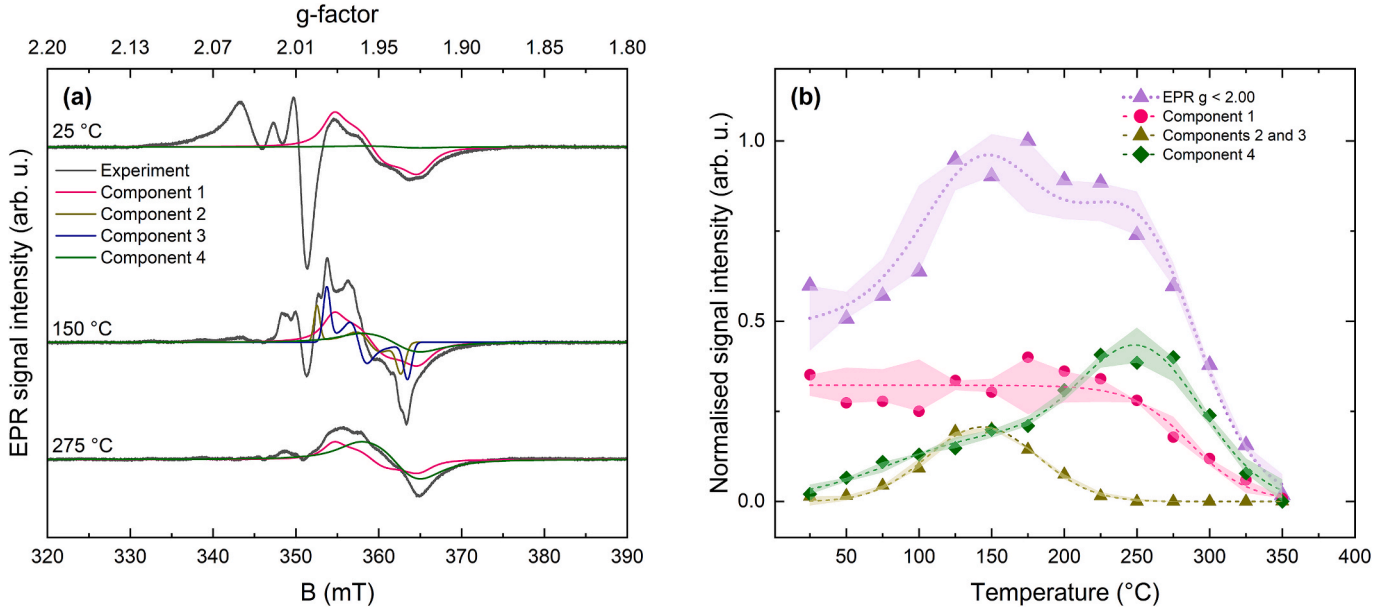

Fig. 8. **(a)** Simulations of radiation-induced $g < 2.00$ signal components after annealing of the thermally pre-treated ACB pebbles at selected temperatures; **(b)** annealing kinetics of individual components constituting the $g < 2.00$ signal.

Table 2
Simulated g-factor values of the ECs in the thermally pre-treated ACB pebbles after irradiation.

Component	g_1	g_2	g_3
1	1.981(2)	1.956(5)	1.926(2)
2	1.993(1)	1.958(5)	1.937(1)
3	1.986(1)	1.965(5)	1.933(1)
4	1.964(2)	1.941(5)	1.924(2)

shown in Fig. 8(a). Their relative contributions to the experimental "EPR $g < 2.00$" spectrum for different annealing temperatures are shown in Fig. 8(b). The errors associated with EPR parameter fitting were minor compared to those introduced by temperature deviations during the annealing process. For Component 1, a three-parameter inverse logit function was used, yielding a PCC value of $r = 0.928$, indicating a satisfactory correlation. Components 2 and 3 displayed nearly identical EPR parameters, annealing behaviours, and intensity profiles. These paramagnetic centres were not detected immediately after irradiation but appeared during annealing. Both were well described by a three-parameter Gaussian distribution, achieving an $r = 0.994$ – an excellent correlation relative to other centres. Component 4, similar to Components 2 and 3, increased in intensity following annealing but exhibited a small initial signal. This suggests that Component 4 may consist of at least two overlapping centres; however, due to its broad linewidth and low initial intensity, further separation was not feasible. It was therefore modelled using a six-parameter double Gaussian distribution, with an $r = 0.978$. The total "EPR $g < 2.00$" intensity was represented as a three-parameter linear convolution of all preceding fits, resulting in an overall $r = 0.972$ for the four-component model – demonstrating a good correlation between the experimental data and the proposed model.

Although unambiguous deconvolution of a broad EPR spectrum into overlapping signals is challenging, several conclusions can be drawn from the obtained simulation results. The g-factor values of the simulated components suggest the presence of a family of structurally related ECs in the thermally pre-treated ACB pebbles after irradiation. The $g < 2.00$ signal structure observed between 25 and 100 °C is primarily governed by the broad Component 1, while at higher annealing temperatures, Component 4 becomes dominant. Components 1 and 4 most likely do not correspond to single, well-defined paramagnetic centre, but rather to distributions of centres exhibiting similar annealing behaviours and broad linewidths. The pronounced signal broadening is attributed to structural disorder, which causes a distribution of g-factor values. Ti → Si substitution in semi-amorphous regions of the Li_4SiO_4 phase could explain a broad distribution of SH parameters. The formation of Components 2 and 3 in the 100–200 °C annealing range is noteworthy, as their powder spectra show better-resolved signal structure. A similar effect was observed in ref. [16] (EPR signal EC(I)), where a gradual transformation between different ECs was proposed. The specific point defects and disorder effects appear to be sample-dependent, as slightly different sets of parameters have been reported in previous studies [16,21]. Consequently, both the material composition and thermal pre-treatment history must be considered when describing charge trapping processes in the pebbles under exposure to ionising radiation.

On the basis of the obtained results, it can be concluded that the formation and accumulation of similar paramagnetic centres occur in the untreated and thermally pre-treated ACB pebbles during irradiation, regardless of the type, mass, or energy of the ionising radiation. Variations in the overall shape and intensity of the experimentally recorded EPR spectra are most likely due to differences in absorbed dose, particle penetration depth within the material, and the time elapsed between irradiation and measurements. The positions of the main peaks in the TSL glow curves during heating up to 250 °C, as well as the stability of the radiation-induced absorption bands, correlate with the decay of the $g = 2.04$ and $g = 2.00$ EPR signals. Within the same temperature range, transformations take place among various electron-type centres, which originate from structurally related sites formed in the bulk of the material. The annealing of these electron-type centres proceeds in multiple stages up to 350 °C, as they recombine with hole-type centres exhibiting different stabilities. Since the onset temperature of tritium release in the neutron irradiated ACB pebbles has been reported at about 300 °C [25], the most thermally stable paramagnetic centres should be taken into account in the analysis of tritium release kinetics. In addition, a colour change from off-white to dark blue-grey was observed for the ACB pebbles under exposure to neutrons at irradiation temperatures below 50 °C, while after TDS measurements up to 900 °C, the dark colouration disappeared, probably due to annealing of radiation-induced colour centres.

4. Conclusions

The formation and accumulation of paramagnetic radiation-induced defect centres was investigated and compared for the first time in the untreated and thermally pre-treated ACB pebbles under exposure to different types of ionising radiation: (1) up to 45 keV X-rays; (2) 10 MeV accelerated electrons; (3) 2.1 MeV H^+ ions. The time interval between irradiation and analysis was identified as a critical factor, as several generated paramagnetic centres are unstable and decay at room temperature. The structure and distribution of stable paramagnetic centres were found to be similar in X-ray and accelerated electron-irradiated pebbles. In contrast, samples irradiated with accelerated ions exhibited a reduced formation efficiency of electron-type centres and a lower overall concentration of paramagnetic centres, primarily due to the limited penetration depth of the ion beam. However, drawing definitive conclusions about the formation mechanisms of paramagnetic centres in the ACB pebbles exposed to different types of ionising radiation is inherently challenging due to the varying interaction mechanisms and the limitations of the spectroscopic methods employed.

The accumulated radiation-induced point defects act as colour centres, resulting in visible colouration of the ACB pebbles. The stability of the radiation-induced absorption bands, as well as the positions of the main peaks in the TSL glow curves, correlates with the decay of the EPR signals at $g = 2.04$ and $g = 2.00$ within the 50–200 °C temperature range. In the same range, transformations take place among various electron-type centres, which originate from structurally related sites formed in the bulk of the material. The annealing of these electron-type centres proceeds in multiple stages up to 350 °C, as they recombine with hole-type centres exhibiting different stabilities. The obtained results highlight the significant role of paramagnetic centres in determining the optical properties of the ACB pebbles. These findings provide a valuable reference framework for interpreting future neutron irradiation experiments of the ACB pebbles, where similar paramagnetic centres and radiation-induced absorption bands are expected to occur under thermonuclear fusion reactor-relevant conditions.

CRediT authorship contribution statement

Andris Antuzevics: Writing – review & editing, Writing – original draft, Visualization, Investigation, Formal analysis, Conceptualization. **Guna Krieke:** Writing – review & editing, Writing – original draft, Methodology, Formal analysis, Conceptualization, Investigation. **Jekabs Cirulis:** Writing – review & editing, Writing – original draft, Investigation. **Magdalena Rzepna:** Writing – review & editing, Resources, Investigation. **Maria Gonzalez:** Writing – review & editing, Resources, Investigation. **Julia M. Leys:** Writing – review & editing, Resources, Investigation. **Regina Knitter:** Writing – review & editing, Resources, Investigation. **Arturs Zarins:** Writing – review & editing, Writing – original draft, Supervision, Resources, Project administration, Investigation, Funding acquisition, Formal analysis, Conceptualization.

Declaration of competing interest

The authors declare that they have no known competing financial interests or personal relationships that could have appeared to influence the work reported in this paper.

Acknowledgements

This work has been carried out within the framework of the EUROfusion Consortium, funded by the European Union via the Euratom Research and Training Programme (Grant Agreement No. 101052200 – EUROfusion), and it has received funding from the Latvian Council of Science, project No. lzp-2024/1-0162 "Influence of stoichiometry on radiation-induced effects in advanced two-phase functional materials for future thermonuclear fusion reactors". Views and opinions expressed are however those of the author(s) only and do not necessarily reflect those of the European Union or the European Commission. Neither the European Union nor the European Commission can be held responsible for them.

Appendix A. Supplementary data

Supplementary data to this article can be found online at https://doi.org/10.1016/j.nme.2025.102035.

Data availability

Data will be made available on request.

References

[1] O. Leys, J.M. Leys, R. Knitter, Current status and future perspectives of EU ceramic breeder development, Fusion Eng. Des. 164 (2021) 112171, https://doi.org/10.1016/j.fusengdes.2020.112171.
[2] L.M. Giancarli, M.-Y. Ahn, S. Cho, Y. Kawamura, A. Leal-Pereira, M. Merola, Y. Poitevin, I. Ricapito, Q. Sheng, H. Tanigawa, H. Tanigawa, J.G. van der Laan, X. Wang, Status of the ITER TBM Program and overview of its technical objectives, Fusion Eng. Des. 203 (2024) 114424, https://doi.org/10.1016/j.fusengdes.2024.114424.
[3] A. Gioè, F.A. Hernández, G. Bongiovì, A. Quartararo, E. Vallone, G. Agnello, G. A. Spagnuolo, S. d'Amico, P. Chiovaro, P.A. Di Maio, Exploratory thermal and fluid-dynamic assessment of a pin of the Helium cooled pebble bed breeding blanket concept with a modular pin monoblock design for the EU DEMO nuclear fusion reactor, Fusion Eng. Des. 218 (2025) 115243, https://doi.org/10.1016/j.fusengdes.2025.115243.
[4] A. Shaimerdenov, J. Leys, T. Kulsartov, D. Sairanbayev, Y. Chikhray, A. Akhanov, S. Askerbekov, M. Ionescu-Bujor, R. Knitter, Rig design development for in situ tritium release studies of EU reference ceramic breeders (ACB-TREND), Fusion Eng. Des. 212 (2025) 114851, https://doi.org/10.1016/j.fusengdes.2025.114851.
[5] T. Kulsartov, Z. Zaurbekova, R. Knitter, I. Kenzhina, Y. Chikhray, A. Shaimerdenov, S. Askerbekov, G. Kizane, A. Yelishenkov, T. Zholdybayev, Comparative analysis of gas release from biphasic lithium ceramics pebble beds of various pebbles sizes and content under neutron irradiation conditions, Nucl. Mater. Energy 38 (2024) 101583, https://doi.org/10.1016/j.nme.2024.101583.
[6] Y. Chikhray, S. Askerbekov, R. Knitter, T. Kulsartov, A. Shaimerdenov, M. Aitkulov, A. Akhanov, D. Sairanbayev, Z. Bugybay, A. Nessipbay, K. Kisselyov, G. Kizane, A. Zarins, Studies of irradiated two-phase lithium ceramics Li_4SiO_4/Li_2TiO_3 by thermal desorption spectroscopy, Nucl. Mater. Energy 38 (2024) 101621, https://doi.org/10.1016/j.nme.2024.101621.
[7] A. Zarins, A. Ansone, M. Senko, J. Cipa, A. Antuzevics, L. Avotina, L. Baumane, G. Kizane, M. Gonzalez, J.M. Leys, R. Knitter, Influence of various radiation types on radiation-induced processes in lithium orthosilicate-based ceramic breeder materials, in: Proceedings of 21st International Workshop on the Ceramic Breeder Blanket Interactions (CBBI-21), 2023, pp. 576–591.
[8] G. Delgado, M. Gonzalez, Secondary Ion Mass Spectrometry (SIMS) as an important tool to track compositional variations from ion-implanted and ion-damaged Advance Ceramic Breeder (ACB) compositions, in: Proceedings of 21st International Workshop on the Ceramic Breeder Blanket Interactions (CBBI-21), 2023, pp. 592–609.
[9] N. Baluc, Materials for fusion power reactors, Plasma Phys. Control Fus. 48 (2006) B165–B177, https://doi.org/10.1088/0741-3335/48/12B/S16.
[10] L.W. Hobbs, F.W. Clinard, S.J. Zinkle, R.C. Ewing, Radiation effects in ceramics, J. Nucl. Mater. 216 (1994) 291–321, https://doi.org/10.1016/0022-3115(94)90017-5.
[11] M.H.H. Kolb, J.M. Heuser, R. Rolli, H.-C. Schneider, R. Knitter, M. Zmitko, The HICU PIE results of EU ceramic breeder pebbles: general characterization, J. Nucl. Mater. 531 (2020) 152023, https://doi.org/10.1016/j.jnucmat.2020.152023.
[12] J. Leys, R. Rolli, H.-C. Schneider, R. Knitter, HICU PIE results of neutron-irradiated lithium metatitanate pebbles, Nucl. Mater. Energy 38 (2024) 101625, https://doi.org/10.1016/j.nme.2024.101625.
[13] A. Iuliano, M. Nowacka, K. Rybak, M. Rzepna, The effects of electron beam radiation on material properties and degradation of commercial PBAT/PLA blend, J. Appl. Polym. Sci. 137 (2020) 48462, https://doi.org/10.1002/app.48462.
[14] M. Siwek, T. Edgecock, A.G. Chmielewski, A. Rafalski, M. Walo, M. Sudlitz, L. Lin, Y. Sun, The potential of electron beams for the removal of microplastics from wastewater and sewage sludge, Environ. Challenges 13 (2023) 100760, https://doi.org/10.1016/j.envc.2023.100760.
[15] A. Redondo-Cubero, M.J.G. Borge, N. Gordillo, P.C. Gutiérrez, J. Olivares, R. Pérez Casero, M.D. Ynsa, Current status and future developments of the ion beam facility at the centre of micro-analysis of materials in Madrid, Eur. Phys. J. Plus 136 (2021) 175, https://doi.org/10.1140/epjp/s13360-021-01085-9.
[16] A. Zarins, A. Antuzevics, G. Kizane, J.M. Leys, R. Knitter, Simulations of complex electron paramagnetic resonance spectra for radiation-induced defect centres in advanced ceramic breeder pebbles, Nucl. Mater. Energy 35 (2023) 101458, https://doi.org/10.1016/j.nme.2023.101458.
[17] A. Antuzevics, A. Zarins, A. Ansone, J. Cipa, G. Kizane, J.M. Leys, R. Knitter, Thermal properties of paramagnetic radiation-induced defects in lithium orthosilicate containing breeder material, J. Nucl. Mater. 565 (2022) 153713, https://doi.org/10.1016/j.jnucmat.2022.153713.
[18] A. Ansone, A. Antuzevics, L. Avotina, E. Sprugis, A. Trimdale-Deksne, J.M. Leys, R. Knitter, A. Zarins, Influence of thermal treatment at various temperatures on structure and radiation-induced effects in advanced ceramic breeder pebbles, Nucl. Mater. Energy 43 (2025) 101944, https://doi.org/10.1016/j.nme.2025.101944.
[19] S. Stoll, A. Schweiger, EasySpin, a comprehensive software package for spectral simulation and analysis in EPR, J. Magn. Reson. 178 (2006) 42–55.
[20] R.I. Mashkovtsev, Y. Pan, Nature of paramagnetic defects in α-quartz: Progresses in the first decade of the 21st century, in: New Developments in Quartz Research: Varieties, Crystal Chemistry and Uses in Technology, 2013, pp. 65–104.
[21] A. Antuzevics, A. Zarins, J. Cirulis, A. Fedotovs, A. Ansone, M. Rzepna, J.M. Leys, R. Knitter, Hyperfine interactions of paramagnetic radiation-induced defect centres in advanced ceramic breeder pebbles, Nucl. Mater. Energy 40 (2024) 101698, https://doi.org/10.1016/j.nme.2024.101698.
[22] J. Cipa, A. Zarins, A. Supe, G. Kizane, A. Zolotarjovs, L. Baumane, L. Trinkler, O. Leys, R. Knitter, X-ray induced defects in advanced lithium orthosilicate pebbles with additions of lithium metatitanate, Fusion Eng. Des. 143 (2019) 10–15, https://doi.org/10.1016/J.FUSENGDES.2019.03.096.
[23] J. Pejchal, V. Babin, A. Beitlerova, S. Kurosawa, Y. Yokota, A. Yoshikawa, M. Nikl, Improvement of the growth of Li_4SiO_4 single crystals for neutron detection and their scintillation and luminescence properties, J. Cryst. Growth 457 (2017) 143–150, https://doi.org/10.1016/j.jcrysgro.2016.02.008.
[24] J.A. Weil, J.R. Bolton, Electron Paramagnetic Resonance, Wiley, 2007.
[25] S. Askerbekov, Y. Chikhray, T. Kulsartov, A. Akhanov, A. Shaimerdenov, M. Aitkulov, Zh. Bugybay, I. Kenzhina, Sh. Gizatulin, R. Knitter, J. Leys, Kinetic analysis of tritium release from irradiated biphasic lithium ceramics Li_4SiO_4-Li_2TiO_3 with different phase ratios, Fusion Eng. Des. 214 (2025) 114873, https://doi.org/10.1016/j.fusengdes.2025.114873.